IEEE Access
Multidisciplinary | Rapid Review | Open Access Journal

Date of publication xxxx 00, 0000, date of current version xxxx 00, 0000.

Digital Object Identifier 10.1109/ACCESS.2017.Doi Number

A Novel Hybrid Image Segmentation Method for Detection of Suspicious Regions in Mammograms Based on Adaptive Multi-Thresholding (HCOW)

Güliz Toz[1], Pakize Erdoğmuş[2]

[1]Computer Technology Department, Karamanoglu Mehmetbey University, Karaman, TURKEY
[2]Department of Computer Engineering, Duzce University, Duzce, TURKEY

Corresponding author: First G. Toz (e-mail: glz.toz@ gmail.com).

ABSTRACT Suspicious region segmentation is one of the most important parts of CAD systems that are used for breast cancer detection in mammograms. In a CAD system, there can be so many suspicious regions determined for a mammogram because of the complex structure of the breast. This study proposes a hybrid thresholding method to use in the CAD systems for efficient segmentation of the mammograms and reducing the number of the suspicious regions. The proposed method provides fully-automatic segmentation of the suspicious regions. This method is based on determining an adaptive multi-threshold value by using three different techniques together. These techniques are Otsu multilevel thresholding, Havrda & Charvat entropy, and w-BSAFCM algorithm that was developed by the authors of this paper for image clustering applications. In the proposed method, segmentation of a mammogram is performed on two sub-images obtained from that mammogram, the pectoral muscle and the breast region to prevent any information loss. The method was tested on 55 mass-mammograms and 210 non-mass mammograms of the mini-MIAS database, and it was compared with Shannon, Renyi, and Kapur entropy methods and with some of the related studies from the literature. The segmentation results of the tests were evaluated in terms of the number of suspicious regions, the number of correctly detected masses, and the performance measure parameters, accuracy, false-positive rate, specificity, volumetric overlap, and dice similarity coefficient. According to the evaluations, it was shown that the proposed method can both successfully locate the mass regions and significantly reduce the number of the non-mass suspicious regions on the mammograms.

INDEX TERMS Breast Cancer, CAD System, Image Segmentation, Thresholding

I. INTRODUCTION

Breast cancer is one of the most important types of cancer that threatens life and results in death among women today. According to the World Health Organization (WHO), 2.3 million women were diagnosed with breast cancer in 2020 and also 685.000 people died from breast cancer in the same year [1]. Therefore, breast cancer treatment is significant in terms of protecting women's health and reducing health expenditures. Early diagnosis of breast cancer is very important since the cases detected at this stage can continue their lives after treatment [2]. Mammography is one of the most common techniques used in breast cancer diagnosis. A radiologist can determine whether a patient has breast cancer or not with the help of mammography. However, there are many factors that affect making decisions difficult in determining abnormalities on the mammograms for the radiologists such as the degree of expertise of the radiologist, the environmental conditions, the structure or the density of the breast, etc. Because of these factors, radiologists fail to notice for 10% to 30% of the cancers [3]. Consequently, in the literature, there are lots of studies performed to help specialists in the detection of breast cancer from mammograms. Most of these studies are called Computer-Aided Diagnosis (CAD) systems. CAD systems can be used for both the detection and classification of cancer types. According to most of the related studies in the literature, it is seen that CAD systems improve the detection process of breast cancer. Moreover, there is no difference between the evaluation of a mammogram using a CAD system and reading of that mammogram by a single radiologist in terms of the sensitivity [4]. On the other hand, when a CAD system is used together with the radiologist as a second reader, the detection rate of cancer is increased [4]. A general CAD system consists of preprocessing, localization and/or segmentation, feature extraction, and classification steps. Exceptionally, in deep learning-based methods, feature extraction, and classification can be combined in a single step [5]. CAD systems can be analyzed in two groups in terms of the evaluated images. The first one is a system in

This article has been accepted for publication in a future issue of this journal, but has not been fully edited. Content may change prior to final publication. Citation information: DOI 10.1109/ACCESS.2021.3089077, IEEE Access

which the images were previously analyzed by a radiologist and the possible cancerous regions were marked. Such a system is considered semi-automatic. In semi-automatic systems, images marked by the radiologist are classified by the CAD system as noncancerous, cancerous, and/or benign or malignant. Some examples of semi-automatic studies can be given as follows: Beura et al. [6] proposed to use GLCM (Gray-Level Co-Occurrence Matrix) and discrete wavelet decomposition for feature extraction and a Feed-Forward Back-Propagation Multilayer Neural Network (BPNN) for classification processes. In another semi-automatic system, Gedik [7] used some coefficients obtained from the Fast Finite Shearlet Transform (FFST) method as features and performed the classification of the images by using the Support Vector Machines (SVM). Wichakam and Vateekul [8] performed mammogram classification using a combination of Convolutional Networks (CN) and SVM on 216 cropped images from the INbreast database. Some of the other studies proposed semi-automatic systems can be found in [9]–[12]. Different from the semi-automatic systems, a fully-automatic CAD system takes the whole of the mammogram image as the input data and performs all the preprocessing and classification processes automatically. Then, it produces the classification results indicating that the mammogram includes mass or not, and/or if there is mass it also shows that the mass is benign or malign. Some examples of these studies are as follows: Lbachir et al. [13] proposed a four-stage automatic CAD system. The first stage is the preprocessing of the images and the abnormal parts of the images are determined by the image segmentation performed using the HRAK algorithm in the second stage. In the third stage, they reduced the false-positives using bagged trees classifier with some of the texture properties and performed the benign and malignant classification using SVM in the last stage. Shrivastava and Bharti [14] performed their study in three phases. In the first phase, the ROIs of the images are automatically determined by a line segmentation method and some preprocessing. Then the mass regions and their sizes are detected using pixel density and the ESRG method in the second phase while the last phase is devoted to the classification. Sheba et al. [15] proposed a method that automatically detects the suspicious regions with global thresholding, the Otsu method, and morphological processes. They used shape, texture, and gray-level properties for feature extraction from the suspicious regions and used Classifier and Regression Tree (CART) to select optimal features. Finally, they proposed a feed-forward artificial neural network using back propagation as the classifier. Some of the other fully-automatic systems can be seen in [16]–[18]. A summary of the semi-automatic and fully-automatic systems presented above is given in Table 1. According to table, it is seen that semi-automatic systems obtained more successful results than fully-automatic systems. One of the reasons behind this result is that the cancerous regions are already determined by an expert and given to the system in a semi-automatic system. In this way, the fact that the cancerous region is directly presented to the system compared to giving the whole mammogram provides decreasing the computation cost while increasing the success rate both in the feature extraction and classification stages. However, it is known that radiologists cannot diagnose 10% to 30% cancers for certain reasons [3]. Therefore, a fully-automatic system will be more useful in helping the radiologist in terms of diagnosis as it can classify the suspicious regions on the whole mammogram. On the other hand, it is very difficult for a system to be fully-automatic because that mammograms are different from each other in many aspects and the system has to make an accurate evaluation despite all of these differences.

TABLE I
SUMMARY OF THE PRESENTED SEMI-AUTOMATIC AND FULLY-AUTOMATIC CAD SYSTEMS FROM THE LITERATURE

Works	Methods	Databases (Image Count)	Performance Measures	Classification Performance
Elmoufidi et al. (2018) [19]	Fully-Automatic	MIAS (115) CBIS-DDSM (500)	Sensitivity Sensitivity	94.78% 95.6%
Lbachir et al. (2020) [13]	Fully-Automatic	MIAS DDSM	Sensitivity Sensitivity	93.15% 90.85%
Sheba et al. (2018) [15]	Fully-Automatic	MIAS (251)	Accuracy	96%
Ballin et al. (2019) [20]	Fully-Automatic	DDSM-BCRP(79) INbreast (116)	Accuracy Accuracy	78%
Shrivastava and Bharti (2020) [14]	Fully-Automatic	MRIRIDER Breast (500) MIAS (322) DDSM (500)	Accuracy Accuracy Accuracy	92.2% 92.6% 90%
Goubalan et al. (2016) [9]	Semi-Automatic	INbreast (48)	Accuracy	98%
Vedanarayanan and Nandhitha (2017) [10]	Semi-Automatic	Centres in Chennai, India (50)	Sensitivity	100%
Beura et al. (2015) [6]	Semi-Automatic	MIAS (322) DDSM (550)	Accuracy Accuracy	98% 98.8%
Lévy and Jain (2016) [12]	Semi-Automatic	DDSM (1820)	Accuracy	92.9%
Gedik (2016) [7]	Semi-Automatic	DDSM (X) MIAS (Y) (X+Y=228)	Accuracy	97.39% 98.29%
Boudraa et al.(2020) [11]	Semi-Automatic	MIAS	Accuracy	96.7%
Wichakam and Vateekul (2016) [8]	Semi-Automatic	INbreast (216)	Sensitivity	100%

One of the most important stages of a fully-automatic system is image segmentation since it directly affects the classification performance of the system and the suspicious regions of the mammograms are determined at this stage. Therefore, many different methods have been presented in the literature for mammogram segmentation. Moghbel et al. [5], presented a review study about mammogram segmentation and performed a classification of these methods. Firstly, they divided the mammogram

This article has been accepted for publication in a future issue of this journal, but has not been fully edited. Content may change prior to final publication. Citation information: DOI 10.1109/ACCESS.2021.3089077, IEEE Access

segmentation studies into two sections as signal-based and model-based segmentations. Then, they divided the modal-based studies into two sub-sections as local and global. Local studies include active contour, level set, graph cut, and Markov Random Fields methods while global studies contain Hough Transform and curve-fitting techniques. Similarly, they examined the signal-based segmentation in two sub-sections, pixel-based and region-based. Region-based studies use region growing, watershed, split and merge, and non-linear filters methods while pixel-based studies utilize linear filters, thresholding, and histogram-based methods. On the other hand, apart from these techniques presented by Moughbel et al. [5], there are some other studies that proposed different image segmentation methods. Some examples can be given as follows; Zebari et al. [21], conducted a hybrid study based on thresholding and machine learning techniques for segmentation of the breast region and pectoral muscle from the mammograms. They used the Histogram of Oriented Gradient (HOG) feature with neural network classifier for determining the region of the pectoral muscle and ROI. They tested their method on mammograms from three different databases and showed that the method obtained an accuracy of 98.13% and 98.41% for the mini-MIAS database, 100%, and 98.01% for INbreast database, and 99.8% and 99.5% for the BCDR database in terms of the detection of the boundary of the breast region and the pectoral muscle segmentation, respectively. Singh et al. [22], firstly used the Single Shot Detector (SSD) for signing the location of the tumor region and then defined a bounding box for that region. Then, they performed the classification by using conditional Generative Adversarial Network (cGAN). They showed that the proposed method provided a high Dice coefficient, 94%, and Intersection over Union (IoU), 87%. Moreover, they classified the generated masks by using Convolutional Neural Network (CNN) into four tumor shapes: irregular, lobular, oval, and round. Patil and Biradar [23], conducted a study on the detection of breast cancer using a fuzzy classifier with an improved region growing algorithm. They optimized the tolerance of region growing and the membership function of the fuzzy logic classifier by the proposed IAP-CSA algorithm. They presented that their method showed better performance than PSO, WOA, and CSA algorithms both for the segmentation and the classification. In another study, Santhos et al. [24], performed several comparisons between various nature-inspired optimization algorithms to obtain the best threshold values for segmentation of the mammograms. They selected the Otsu and Kapur methods as the objective functions and compared the performances of the algorithms according to these functions. As the result, they found that McCulloch's algorithm that inspired by the Cuckoo Search Optimization algorithm (MACSO), together with the Otsu thresholding as the objective function, obtained the best results in the segmentation of the mammograms. Kaitouni et al. [25] aimed to eliminate the pectoral muscle and segment the masses from mammograms. They firstly performed thresholding by the Otsu method for the elimination of the artifacts and then estimated a number for the base classes by using the local binary pattern. Then, they proposed an improved k-means algorithm by using the Markov method for the classification and determined the class that includes the tumor and pectoral muscle by considering the correlation between the classes and the original image. Finally, they used the region growing method to eliminate the pectoral muscle. Gupta and Tiwari [26] developed a software tool for helping radiologists in the segmentation of mammograms. The tool was based on a method named histogram modified gray relational analysis proposed by the authors. Their method segments the breast region by improving the local and global contrasts of a given mammogram image. They showed the effectiveness of their tool by examining 322 mammograms from the mini-MIAS database. On another side, there are deep learning-based techniques in the literature for mammogram segmentation. Ahmed et al. [27] used DeepLab and Mask RCNN as deep learning models in their study for both the extraction of the pectoral muscle and mass segmentation. They tested their method on the images taken from the mini-MIAS and CBIS-DDSM databases and showed that they achieved 95% classification success for DeepLab and 98% for Mask RCNN. Al-antari et al. [28] proposed a study based on deep learning for breast mass detection, segmentation, and classification. Firstly, they used You-Only-Look-Once (YOLO) deep learning approach for mass detection. Secondly, they proposed and utilized full resolution convolutional network for mass segmentation. Finally, they used a deep CNN for mass classification (benign vs. malignant) and used the INbreast database to evaluate the proposed integrated CAD system in terms of the accuracies of detection, segmentation, and classification. The evaluation results of the proposed CAD system via four-fold cross-validation tests showed a mass detection accuracy of 98.96%, Matthews correlation coefficient (MCC) of 97.62%, and F1-score of 99.24%.

Considering all these presented methods from the literature, it is seen that there is no single segmentation method that can be successfully applied to all mammograms. Moreover, it is also seen that each method has its own challenges. In the deep learning-based techniques too many images and a large memory space are required. In the region growing-based methods, it is necessary to give the location and color information of the seeds manually or perform extra processes for determining these values. On the other hand, in the global thresholding-based methods, obtaining a suitable threshold value for tumor segmentation is difficult due to the different nature of mammograms. And, local thresholding is costly in terms of the processing load because of the separate processing of each region of the mammogram.

By considering these problems, in this study, a method based on an adaptive multi-thresholding technique was proposed. The proposed method was composed by using three different techniques together. These techniques are

This article has been accepted for publication in a future issue of this journal, but has not been fully edited. Content may change prior to final publication. Citation information: DOI 10.1109/ACCESS.2021.3089077, IEEE Access

Otsu multilevel thresholding [29], Havrda & Charvat entropy [30], and the w-BSAFCM algorithm [31] that was proposed by the authors of this paper for image clustering applications and based on the BSA [32] and FCM [33] algorithms. With the help of these three techniques fully automatic selection of the suspicious regions from the mammograms for breast cancer diagnosis was provided. The effectiveness of the method was tested in two manners; firstly, its performance on the mass-mammogram segmentation was tested on 55 mass-mammograms from the mini-MIAS database [34]. And, secondly, 210 normal mammograms were segmented by the proposed method. The obtained results were compared with three well-known methods from the literature; Shannon [30], Renyi [30], and Kapur entropies [30] and also with the results obtained from some of the related studies in the literature. The number of suspicious regions and the number of correct masses detected were calculated from the obtained results for evaluation purposes. Also, the performance indices, volumetric overlap, dice similarity coefficient, accuracy, false-positive rate and specificity were calculated using pixel values over the detected suspicious regions to demonstrate the effectiveness of the proposed method and presented in comparison with the other methods.

The remaining parts of the paper were organized as follows: The proposed image segmentation method explained in detail in the second section. The experimental studies and their results were presented in the third section. And, the paper was concluded in the last section.

II. PROPOSED IMAGE SEGMENTATION METHOD

Image segmentation is an important part of the fully-automatic CAD systems. For a mammogram, image segmentation aims to determine the suspicious regions of the mammogram to make the system get a more successful classification result. This section presents the proposed hybrid image segmentation method in detail. Firstly, preprocessing that purposes to make the image ready for further processing was performed.

A. PREPROCESSING

Preprocessing of the mammograms was performed in several sub-processes. In the first step, the breast region on the mammogram was segmented both to determine the region of interest and to eliminate the artifacts on the mammogram. Then, the noises on the image were removed. There are different methods in the literature for reduction the distorting effects of the noise, according to the characteristics of the image and the frequency and statistical distribution of the noise [35]–[37]. In this study, spatial and transform domain-oriented methods were used together for the noise reduction. In the spatial domain, a 3×3 median filter and in the transform domain a biorthogonal wavelet transform 3.5 were used. The second method applied to the image after the noise reduction is image enhancement. In the literature, there are many different techniques applied for image enhancement [37]–[40]. We used a frequently preferred technique in the literature for image enhancement, namely contrast-limited adaptive histogram equalization (CLAHE) [41]. In CLAHE, the image is divided into small regions that are nearly equal in size and non-overlapping each other. We used anisotropic diffusion [42] to remove the noises on the regions determined by the CLAHE. In the anisotropic diffusion method, the image noise is reduced while preserving important parts of the image, such as lines, edges, or other details important for the interpretation of the image [35]. The flowchart drawn for the performed preprocessing is given in Figure 1 with a sample image.

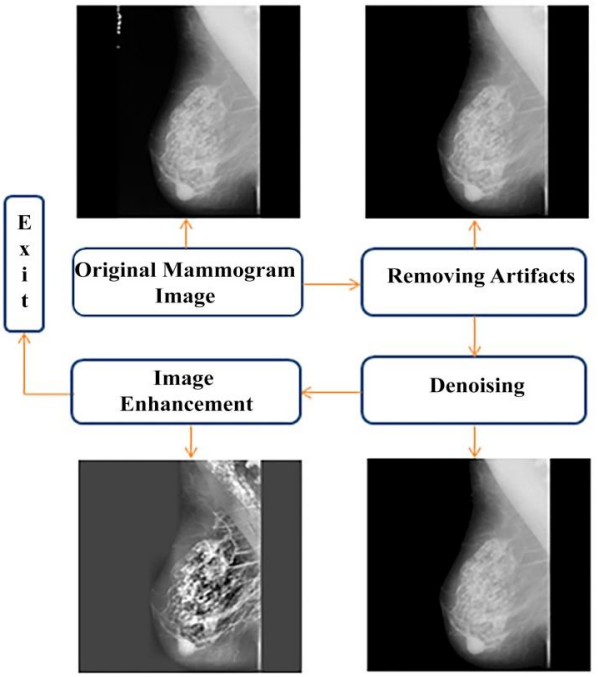

FIGURE 1. Flowchart of the preprocessing with a sample image

B. DETERMINATION OF SUSPICIOUS REGIONS

Every stage of a CAD system is important for the correct diagnosis of abnormalities. Identifying suspicious regions is one of the most important of these stages since the system will be working on these regions during the whole process. These regions are candidates to be mass or calcification and abnormalities are determined over these regions in the next stages. On the other hand, finding an automated, accurate, and efficient suspicious regions segmentation technique in digital mammography is still a challenge today [43]. In the literature, there are lots of studies performed to the determination of these regions from the mammograms [43]–[48]. In this study, a suspicious region determination method that is based on an adaptive multi-thresholding technique was proposed. This method is based on the Otsu multilevel thresholding, Havrda & Charvat entropy, and an image clustering algorithm w-BSAFCM that was proposed by the authors of this paper. In the following sub-sections, these techniques were presented.

This article has been accepted for publication in a future issue of this journal, but has not been fully edited. Content may change prior to final publication. Citation information: DOI 10.1109/ACCESS.2021.3089077, IEEE Access

1) OTSU MULTILEVEL THRESHOLDING

Otsu multilevel thresholding is a global thresholding method proposed by Nobuyuki Otsu [29]. In this method, automatic thresholding is performed by using zero and first-order cumulative moments of the gray-level histogram [44]. Let $[0,1,2,\dots,G_L-1]$ be the gray levels of an $M \times N$ input image, n_i be the pixel number of the i'th gray value and assume that a threshold value, O_t, $0 < O_t < G_L - 1$ is selected to separate the image into two regions as C_1 and C_2. In this case, the C_1 and C_2 classes include the pixels having intensity values in $[0, O_t]$ and $[O_t + 1, G_L - 1]$ ranges, respectively. Then, the probability of the C_1 and C_2 classes, can be calculated as follows, respectively [43]:

$$P_1(O_t) = \sum_{i=0}^{O_t} pi \quad (1)$$

$$P_2(O_t) = \sum_{i=O_{t+1}}^{G_L-1} pi = 1 - P_1(O_t) \quad (2)$$

Where p_i is the probability of i'th pixel in the related class. The mean intensity values of C_1 and C_2 and the global mean intensity value of the image can be defined using Equations 3-5, respectively [43]:

$$m_{c1}(O_t) = \frac{1}{P_1(O_t)} \sum_{i=0}^{O_t} ip_i \quad (3)$$

$$m_{c2}(O_t) = \frac{1}{P_2(O_t)} \sum_{i=O_t+1}^{G_L-1} ip_i \quad (4)$$

$$m_G = \sum_{i=0}^{G_L-1} ip_i \quad (5)$$

The optimum threshold value is O_t^* that maximizes the following criterion or equivalently $\sigma_B^2(O_t)$ [43]:

$$y(O_t) = \frac{\sigma_B^2(O_t)}{\sigma_G^2} \quad (6)$$

Where, $\sigma_B^2(O_t)$ and σ_G^2 are the variance between the classes and the global variance, respectively, and defined by the following equations [43]:

$$\sigma_B^2(O_t) = P_1(m_{c1} - m_G)^2 + P_2(m_{c2} - m_G)^2 \quad (7)$$

$$\sigma_G^2 = \sum_{i=0}^{G_L-1} (i - m_G)^2 P_i \quad (8)$$

Finally, the optimum threshold value, O_t^* is obtained.

In this study, Otsu multilevel thresholding was used to find four optimum threshold values, O_{t1}^*, O_{t2}^*, O_{t3}^*, and O_{t4}^*. The formulations to find these values considering the Equations 1-8 can be written as follows [49]:

$$P_1 = \sum_{i=0}^{O_{t1}} p_i \quad (9)$$

$$P_2 = \sum_{i=O_{t1+1}}^{O_{t2}} pi \quad (10)$$

$$P_3 = \sum_{i=O_{t2+1}}^{O_{t3}} pi \quad (11)$$

$$P_4 = \sum_{i=O_{t3+1}}^{O_{t4}} pi \quad (12)$$

$$P_5 = \sum_{i=O_{t4+1}}^{G_L-1} p_i \quad (13)$$

$$m_{c1} = \frac{1}{P_1} \sum_{i=0}^{O_{t1}} ip_i \quad (14)$$

$$m_{c2} = \frac{1}{P_2} \sum_{i=O_{t1+1}}^{O_{t2}} ip_i \quad (15)$$

$$m_{c3} = \frac{1}{P_3} \sum_{i=O_{t2+1}}^{O_{t3}} ip_i \quad (16)$$

$$m_{c4} = \frac{1}{P_4} \sum_{i=O_{t3+1}}^{O_{t4}} ip_i \quad (17)$$

$$m_{c5} = \frac{1}{P_5} \sum_{i=O_{t4+1}}^{G_L} ip_i \quad (18)$$

Using these equations the between-class variance can be defined as follows:

$$\sigma_B^2(O_{t1}, O_{t2}, O_{t3}, O_{t4}) = P_1(m_{c1} - m_G)^2 + P_2(m_{c2} - m_G)^2 + P_3(m_{c3} - m_G)^2 + P_4(m_{c4} - m_G)^2 \quad (19)$$

The optimum thresholds are the $O_{ti} = (1,2,3,4)$ values that maximize Equation 19 [49].

$$\sigma_B^2(O_{t1}^*, O_{t2}^*, O_{t3}^*, O_{t4}^*) = max\sigma_B^2(O_{t1}, O_{t2}, O_{t3}, O_{t4}) \quad (20)$$

2) HAVRDA & CHARVAT ENTROPY

Entropy is the randomness in the intensity distribution [49]. The more organized a system is, the lower its information entropy; on the contrary, the more complex the system is the higher the information entropy. The following equation defines the amount of information having by a random event G that occurs with the probability $P(G)$ [30].

$$I(G) = log[1/P(G)] = -log[P(G)] \quad (21)$$

Where $I(G)$ is the self-information of the event and there is an inverse ratio between $P(G)$ and $I(G)$. Let the probability distribution of a discrete source be defined by $p_1, p_2, p_3, \dots, p_i, \dots, p_k$. Where, $0 \le p_i \le 1$, $\sum_{i=1}^{k} p_i = 1$ and k is the total number of states. Accordingly, Havrda & Charvat entropy can be defined from the probability distribution as in Equation 22 [30].

$$HC = \frac{1}{1-\alpha} \left(\sum_{i=0}^{k} {p_i}^{\alpha} - 1 \right) \alpha \neq 1, \alpha > 0 \quad (22)$$

Where α is a reel positive number. Mammograms can be examined in three sections in terms of the Havrda & Charvat entropy as breast tissue region, suspicious region, and background. The background does not contain any information useful for diagnosis and can be excluded. The following equation can be used to both find an average gray level value, k, for the breast tissue and excluding the background [30].

$$k = \frac{1}{n} \sum_{i,j \in R}^{M} \sum_{i,j \in R}^{N} f(i,j) \quad (23)$$

Where, M and N are the mammogram dimensions, R is a threshold value that is used for determining the pixels that belong to the breast tissue, n is the number of these pixels and $f(i,j)$ is the gray value at (i,j) coordinates of the ROI [30]. In the literature, generally, R was selected as a constant number such as $R \ge 100$ [30], [49]. On the other hand, the differences in mammogram image quality such as sharpness, contrast, exposure, etc. can affect the accuracy in the

This article has been accepted for publication in a future issue of this journal, but has not been fully edited. Content may change prior to final publication. Citation information: DOI 10.1109/ACCESS.2021.3089077, IEEE Access

diagnosis of breast cancer [50]. Therefore, an adaptive R value that is automatically determined according to the properties of the mammogram will be more efficient for a fully-automatic system. So, in this study, we proposed to adaptively determine the R value considering the properties of the handled mammogram to prevent possible information loss. This value was calculated by using the Otsu multilevel thresholding as given in Equation 24 and named as $Otsu_{thr}$. $Otsu_{thr}$ is a mammogram-specific threshold value for separation of the background and the breast tissue.

$$Otsu_{thr} = \varphi O_{t2}^{*} + \Phi O_{t3}^{*} \quad (24)$$

Where O_{t2}^{*} and O_{t3}^{*} are the second and third optimum threshold values computed by Equation 20. And, φ and Φ are two constant numbers that experimentally determined as 0.55 and 0.45, respectively. After determining the adaptive R value, in Havrda & Charvat entropy method, the probability distribution can be defined as follows; Let $p_1, p_2, \ldots, p_{k-1}, p_k, p_{k+1}, \ldots\ldots, p_L$ be the probability distribution of a mammogram where p_k is the normalized histogram of the mammogram and calculated as given in Equation 25 [30].

$$p_k = h_k/(MxN) \quad (25)$$

Where, h_k is the gray level histogram of the mammogram. According to these definitions probability distribution of the three regions, background, breast tissue, and suspicious region can be written as follows [30]:

The probability distribution of the background:

$$\frac{p_1}{P_{k-1}}, \frac{p_2}{P_{k-1}}, \ldots\ldots\ldots, \frac{p_{k-1}}{P_{k-1}}$$

The probability distribution of the breast tissue:

$$\frac{p_k}{P_t - P_{k-1}}, \frac{p_{k+1}}{P_t - P_{k-1}}, \ldots\ldots\ldots, \frac{p_t}{P_t - P_{k-1}}$$

The probability distribution of the suspicious regions:

$$\frac{p_{t+1}}{1-P_t}, \frac{p_{t+2}}{1-P_t}, \ldots\ldots\ldots\ldots, \frac{p_L}{1-P_t}$$

In the equations, $P_{k-1} = \sum_{i=1}^{k-1} p_i$, $P_t = \sum_{j=1}^{t} p_j$ and t is the candidate threshold value for the suspicious regions, while L is the maximum gray value of the mammogram [30].

According to these distributions, Havrda & Charvat entropy of the breast tissue, $HC_{DB}(t)$ and of the suspicious regions $HC_{ROI}(t)$ for t are defined as follows:

$$HC_{DB}(t) = \frac{1}{1-\alpha}\left[\sum_{i=k}^{t}\left(\frac{p_i}{P_t - P_{k-1}}\right)^{a} - 1\right] \quad (26)$$

$$HC_{ROI}(t) = \frac{1}{1-\alpha}\left[\sum_{i=t+1}^{L}\left(\frac{p_i}{1-P_t}\right)^{a} - 1\right] \quad (27)$$

Finally, the optimum threshold value t_{opt}^{HC} by using Havrda & Charvat entropy can be determined as follows [30]:

$$t_{opt}^{HC} = Arg_{t=k}^{L} \max[HC_{DB}(t) + HC_{ROI}(t) + (1-\alpha)HC_{DB}(t)HC_{ROI}(t)] \quad (28)$$

Where α is a constant value that dynamically defined for each image as explained in [49]. In this study α was calculated as $\alpha = 1 - (k/255)$.

3) W-BSAFCM ALGORITHM

The last method used in this study for thresholding is the w-BSAFCM algorithm. This algorithm was proposed by the authors of the present study for image clustering applications [31]. w-BSAFCM is based on the BSA [32] and FCM [33] algorithms. The authors combined these two algorithms and used an inertia weight parameter (w) to improve its clustering performance. Details of this algorithm can be found in [31]. In this study, w-BSAFCM was used to cluster the mammograms into four clusters and the center that has the highest gray level value among these centers was determined as $wbsafcm_h$.

4) PROPOSED HCOW (**H**AVRDA & **C**HARVAT, **O**TSU, **W**-BSAFCM) METHOD FOR SUSPICIOUS REGION DETERMINATION

In a mammogram, a very large area of the image is composed by the background that is not related to the breast tissue. On the other hand, mass-like structures have higher gray level values than the average gray level value of the breast region. Although the histogram of the image supplies the information about the gray level distribution of the mammogram, this information is not sufficient for mass detection.

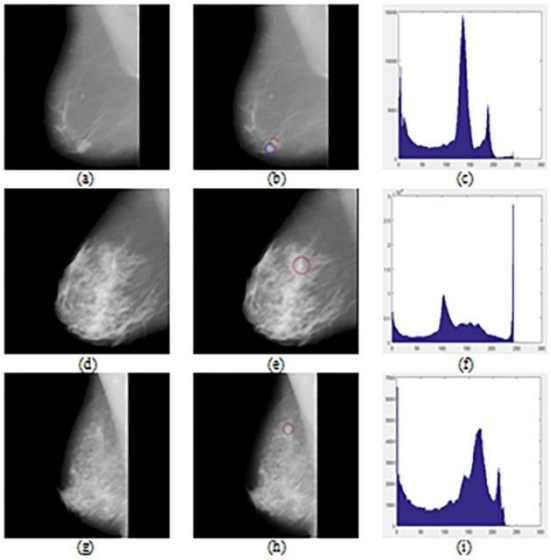

FIGURE 2. Sample images to show the differences between the mammograms. Original mammograms (a, d, g), the masses depicted by circles on the mammograms (b, e, h), and the histogram graphics of the original mammograms (c, f, i).

Figure 2 (a, d, g) shows 3 mammograms with different breast structures (dense, fatty). The mass regions of these images were marked in Figure 2 (b, e, h) and their histogram graphics were depicted in Figure 2 (c, f, i). It should be noted that the zero values are not considered in the histogram graphics. When Figure 2 is examined, it can be seen that while it is easy to distinguish the mass regions for some mammograms such as 2 (a) it is more difficult for some of

This article has been accepted for publication in a future issue of this journal, but has not been fully edited. Content may change prior to final publication. Citation information: DOI 10.1109/ACCESS.2021.3089077, IEEE Access

the others 2 (d, g). For example, in Figure 2 (d, e and g, h), it is seen that the structure of the mass and some other parts of the breast area show similar characteristics.

One of the most important points that should be taken into account about MLO mammograms is the existence of the pectoral muscle. Since the pectoral muscle shows similar characteristics with the masses and other abnormal structures, it is confused with suspicious areas in CAD systems and this makes accurate diagnosis difficult [51]. Therefore, many researchers have preferred to remove the pectoral muscle. The pectoral muscle segmentation is still a challenge as the shape, size and density values of mammograms differ from mammogram to mammogram. Therefore, many different methods have been developed for the segmentation of the pectoral muscle [52]–[55]. On the other hand, some mammograms may also have mass in the pectoral muscle area. Thus, completely removing the pectoral muscle from a mammogram may cause loss of information. For this reason, in this study, the pectoral muscle was segmented and examined separately from the breast area instead of removing it.

It is clear that determining an ideal threshold value that can be used for the successful segmentation of all the mammograms is very difficult. Considering this fact, this study proposes to use image-specific threshold values instead of a general threshold value. Thus, the segmentation process of each mammogram can be performed according to the threshold values that were determined by using only its self-characteristics. In this study, it is proposed to use two image-specific threshold values for each mammogram, one for the pectoral muscle and one for the breast region. Hence, the pectoral muscle should be obtained before the suspicious regions segmentation processes. To obtain the pectoral muscle of a mammogram, firstly, four threshold values were determined for the whole mammogram using the Otsu multilevel thresholding method [29], and the highest of these values was used to convert the image into binary form. Then, with the help of the morphological operators and some logical queries the pectoral muscle was obtained. After determining the pectoral muscle region, the mammogram can be handled as two sub-images, the pectoral muscle and the breast region. These two images can be segmented for the suspicious regions, separately. And, the results of the two segmentation processes can be combined to obtain the suspicious regions of the whole mammogram.

In this study, the three different techniques, explained in the previous section, were used together and a novel method called HCOW for suspicious region determination of the mammograms was introduced. It should be noted that, the proposed method was applied in the same manner to find the both of the threshold values. The HCOW method can be explained step by step as follows;

A_1. In this step, preprocessing is applied to the mammogram image as explained in Section A. Preprocessing operations are removal of artifacts and labels in mammogram, noise removal and image enhancement, in order. Then, the image is divided into two sub-images, the pectoral muscle and the breast region. After this first step, the following steps are applied to two sub-images, separately.

A_2. Four threshold values are obtained by using the Otsu multilevel thresholding method for the preprocessed image, as explained in Equations (9-20).

A_3. The $Otsu_{thr}$ value is calculated as given in Equation 24 by using the second and third threshold values obtained in A_2 step.

A_4. The k value in Equation 23 is calculated by equating the R value in that equation with the $Otsu_{thr}$ value obtained in A_3 step.

A_5. t_{opt}^{HC} is calculated by using the k value from the previous step and the α value ($\alpha = 1 - (k/255)$).

A_6. The preprocessed image is clustered into four clusters using w-BSAFCM algorithm and the center that has the highest gray level value is determined as the $wbsafcm_h$ to use in Equation 29.

A_7. Using Equation 29 the final threshold value, $HCOW_{thr}$, is calculated.

$$HCOW_{thr} = \delta t_{opt}^{HC} + \lambda wbsafcm_h \quad (29)$$

Where δ and λ are two constant values experimentally determined as $\delta = 0.65$ and $\lambda = 0.35$, respectively.

A_8. In this step, the preprocessed image is converted into the binary form by using the $HCOW_{thr}$ threshold value.

A_9. As the last step, the morphological operators are used to remove the remained very small regions that cannot be a mass on the binary image.

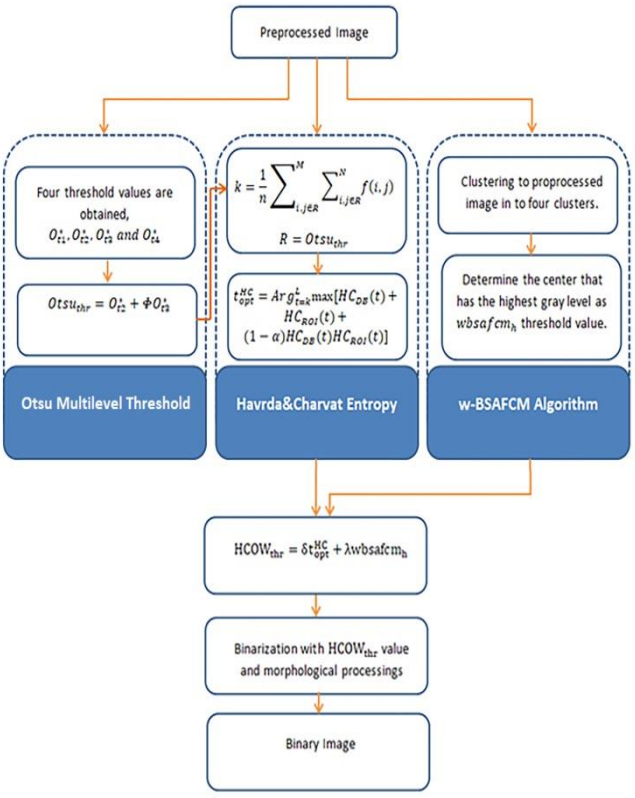

FIGURE 3. Flowchart of the HCOW method.

This article has been accepted for publication in a future issue of this journal, but has not been fully edited. Content may change prior to final publication. Citation information: DOI 10.1109/ACCESS.2021.3089077, IEEE Access

The flowchart of the proposed HCOW method is presented in Figure 3.

By finding the two different threshold values for the same mammogram, it is guaranteed to perform the segmentation of the suspicious regions for the entire mammogram. Then, all the obtained suspicious regions are combined to produce the final set of the suspicious regions for that mammogram. This process is presented in Figure 4. As can be seen from the figure, the original mammogram firstly divided into two sub-images as explained before, the pectoral muscle and the remaining part and then the preprocessing is performed. Then, the HCOW method is applied to the two preprocessed images, separately. After that, the images are converted to the binary form by using the two calculated threshold values, and the suspicious regions are obtained by using some morphological operators on the binary images. Finally, all the obtained suspicious regions are combined to create the final set of the suspicious regions for the related mammogram.

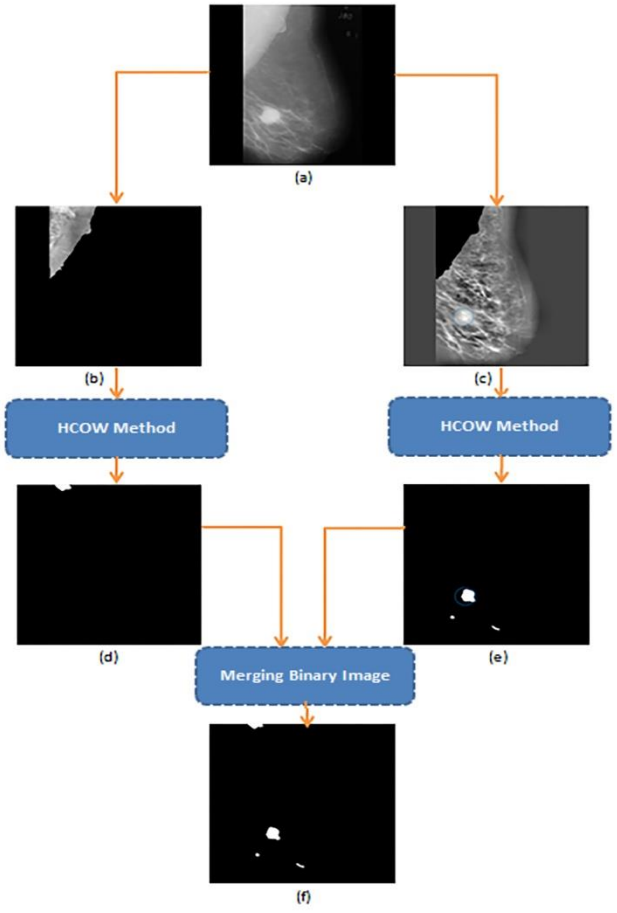

FIGURE 4. Application of the HCOW method to a mammogram Image. (a) Original mammogram, (b) Preprocessed pectoral muscle region, (c) Preprocessed breast region without pectoral muscle, (d) ROI for the pectoral muscle, (e) ROI for the breast region without pectoral muscle, (f) Merging binary images.

To visually show the results of the proposed algorithm on the mammograms, four images from mini-MIAS database are given as examples in Figure 5. In the figure ground truths of the mass regions determined by the radiologist are marked by using blue color circles. From the figure it can be seen that the proposed method successfully finds the mass regions, while reducing the non-mass regions that can significantly affect the classification performance of a fully-automatic CAD system.

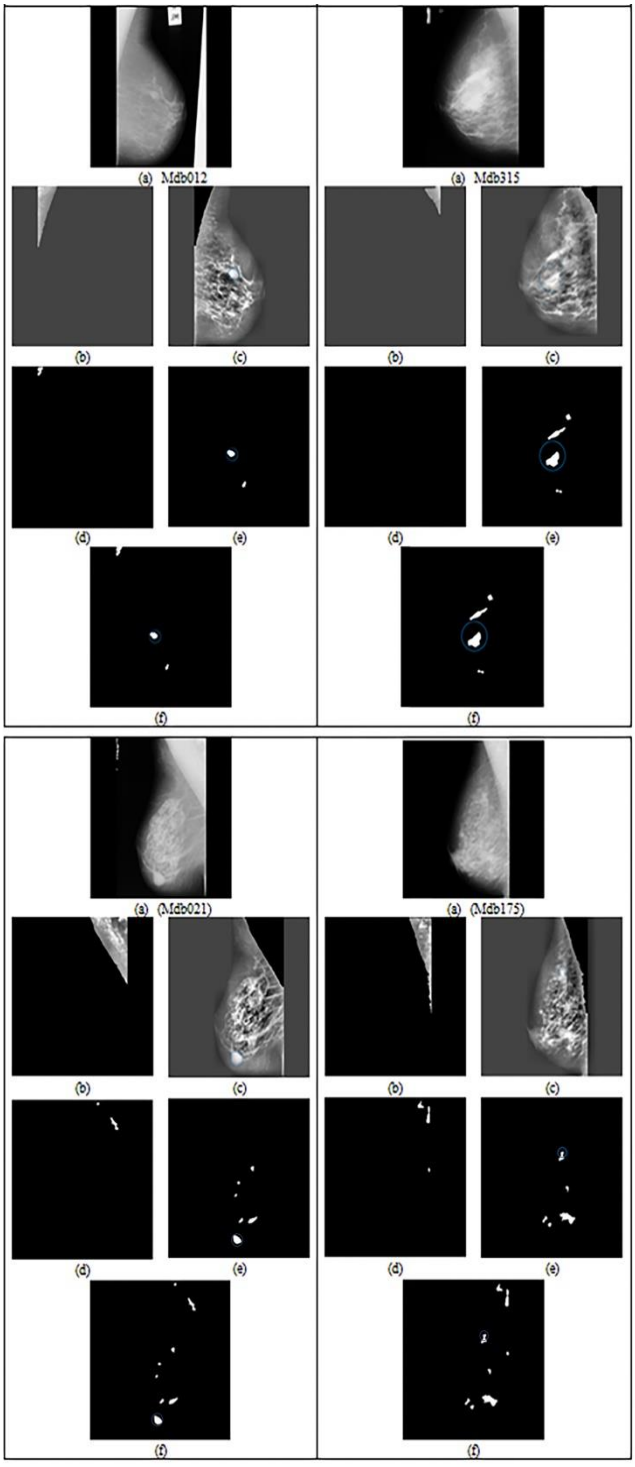

FIGURE 5 Four sample images and their suspicious regions determined by the HCOW method. (a) Original mammogram (b) Preprocessed pectoral muscle region (c) Preprocessed breast region without pectoral muscle (d) ROI of pectoral muscle (e) ROI of the breast region without pectoral muscle (g) merging two binary images

This article has been accepted for publication in a future issue of this journal, but has not been fully edited. Content may change prior to final publication. Citation information: DOI 10.1109/ACCESS.2021.3089077, IEEE Access

III. EXPERIMENTAL STUDIES

In this section, the effectiveness of the HCOW method was presented by using three different experiments performed on the mammograms taken from the mini-MIAS database [34]. The obtained results were compared with the Renyi, Kapur, and Shannon entropy methods and also with the results obtained from some of the recently published studies in the literature.

In the mini-MIAS database, there are 56 mass mammograms, one of these mammograms has no ground truth and three of them have two masses. Therefore, the experiments were performed on 58 masses.

Noise reduction was used to reduce the distorting effects on the image. Thus, the aim of the first experiment is to test the performance of the applied noise reduction techniques. To this end, firstly the HCOW method was utilized for the original forms of the mass mammograms (without noise reduction) and then the same operation was performed for the mammogram images obtained after the noise reduction process. The numbers of the accurately determined mass regions and of the obtained suspicious regions in these two processes are given in Table II.

TABLE II.
THE NUMBERS OF THE ACCURATELY DETERMINED MASS REGIONS AND OF THE OBTAINED SUSPICIOUS REGIONS WITH AND WITHOUT THE NOISE REDUCTION.

METHODS	HCOW (with noise reduction)	HCOW (without noise reduction)
The number of masses that accurately found	**56**	52
The number of masses that cannot be found	**2**	6
The number of suspicious regions incorrectly determined as mass	**358**	363

According to the table, it is seen that when the noise reduction methods are applied to mammogram images, the more masses and the less number of suspicious regions determined by the HCOW method compared with the test that performed without the noise reduction.

In the second experiment, the performance of the proposed method in determining the mass regions was tested. This test was also performed by Shannon, Renyi, and Kapur entropy methods, and the obtained results were compared with each other. It should be noted that, except for calculating the threshold values, other processes were applied in the same way, in the same order, and under the same conditions for all the methods.

Firstly, the effect of using the proposed adaptive R value instead of a constant value is visually presented. The suspicious regions obtained by using $R \geq 100$ and $R \geq Otsu_{thr}$ for five sample images for all the methods are given in Figures 6 and 7, respectively. In the figures, the ground truths of the mass regions are marked by using blue and red circles.

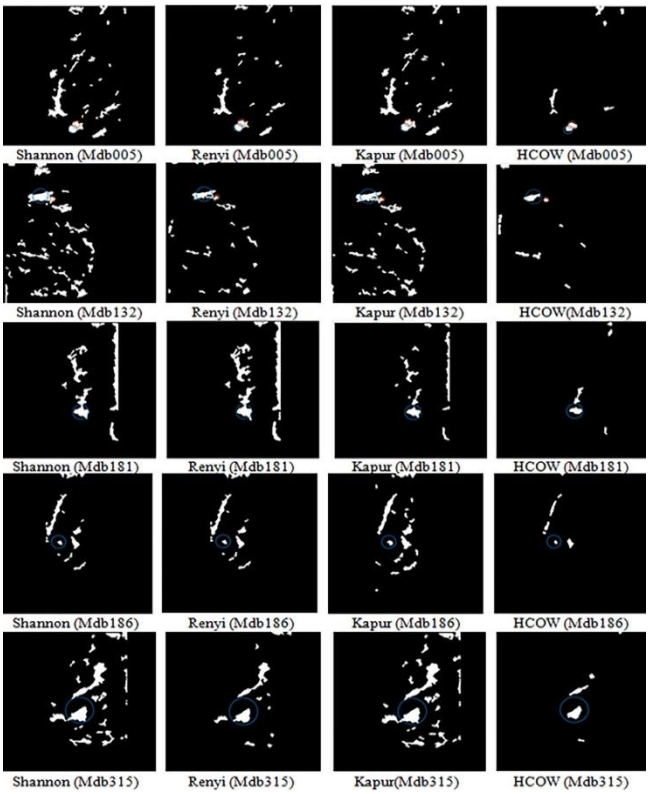

FIGURE 6 Suspicious regions found by using $R \geq 100$ for all the methods

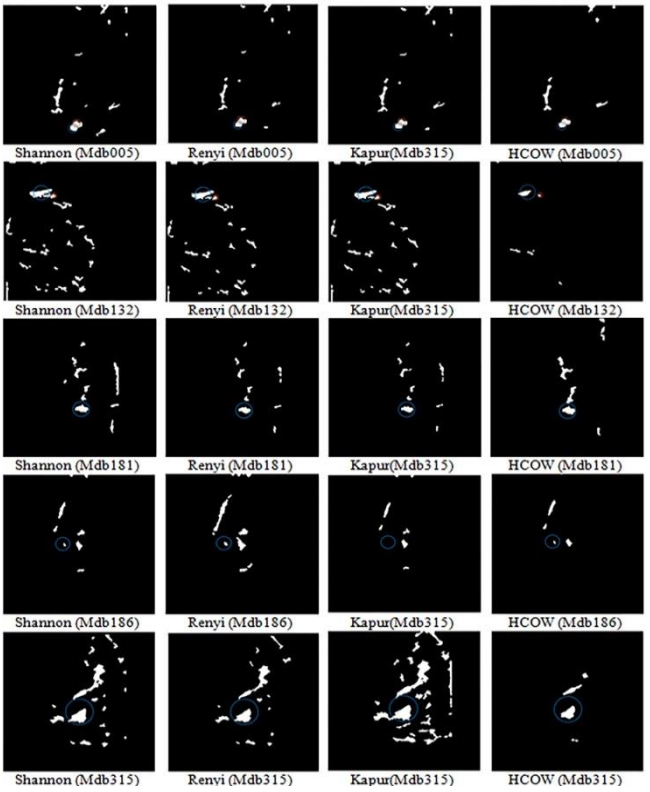

FIGURE 7 Suspicious regions found by using $R \geq Otsu_{thr}$ for all the methods

This article has been accepted for publication in a future issue of this journal, but has not been fully edited. Content may change prior to final publication. Citation information: DOI 10.1109/ACCESS.2021.3089077, IEEE Access

According to Figures 6 and 7, it is seen that the proposed method produces much better results than Kapur, Renyi, and Shannon entropy methods when evaluated in terms of both finding the real mass regions and in reducing the number of non-mass areas. In addition, it can be seen that the suspicious regions found by the HCOW method have similar properties with the masses in terms of shape and size. This provides obtaining more accurate results in the detection of the mass on the mammogram. On the other hand, a lot number of suspicious regions found by the other methods show different characteristics than the mass regions and this causes reducing the accurate diagnosis rate of the system while increasing the computational cost.

In this study, the aim of determining suspicious regions for a mammogram is to find the location and size of the mass on that mammogram. Because, the determined suspicious regions will be cropped and examined to decide that if they are cancerous or non-cancerous in the next stage of the fully-automatic CAD system. Therefore, as the area size of the suspicious regions and their integration with each other are increasing the accurate classification performance of the system will decrease.

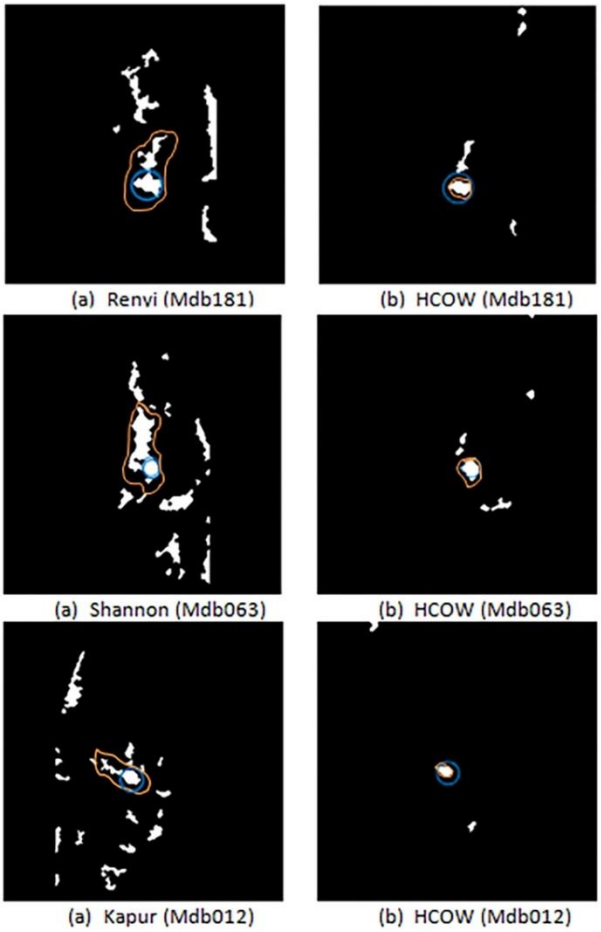

FIGURE 8 Mass and non-mass regions integration in the suspicious regions (a) Kapur, Renyi and Shannon methods (b) The HCOW method (orange curve : the regions found by the algorithms; blue circle: the ground truths)

To exemplify the mass and suspicious regions integration four images are given in Figure 8. In the figure, the ground truths of the mass regions are shown by blue circles while the mass regions that found by algorithm, are depicted by the orange curves. According to the figure, it can be seen that the sizes of the suspicious regions obtained by the Shannon, Renyi, and Kapur entropy techniques are greater several times than the size of the real masses. In other words, the mass regions could not be detected effectively and many unnecessary areas around the masses are also found as suspicious regions. On the other hand, the sizes of the suspicious regions determined by the HCOW method are about the same sizes as the real mass regions given in the ground truths. Moreover, in the figure, it can be seen that the mass regions are integrated with non-mass areas in the results obtained by the Kapur, Renyi, and Shannon methods while the HCOW method successfully located the mass regions as being separated from the other suspicious regions. Such integrations may cause reduce the success of the classification algorithm of the system since the suspicious regions will be taken into account as a whole for the classification process.

One of the most important issues in mass detection is the correct identification of the mass and this is closely related to the number of determined suspicious regions. The higher the number of the suspicious regions, the more difficult determination of the real mass. Therefore, the numbers of the suspicious regions obtained in the experiments for $R \geq 100$ and $R \geq Otsu_{thr}$ are given in Tables 3 and 4, respectively.

TABLE III
THE NUMBERS OF THE SUSPICIOUS REGIONS OBTAINED FOR $R \geq 100$

Thresholding methods	The number of masses that accurately found	The number of masses that cannot be found	The number of suspicious regions incorrectly determined as mass
HCOW	**55**	**3**	**389**
Renyi	55	3	858
Kapur	55	3	963
Shannon	54	4	1030

TABLE IV
THE NUMBERS OF THE SUSPICIOUS REGIONS OBTAINED FOR $R \geq Otsu_{thr}$

Thresholding methods	The number of masses that accurately found	The number of masses that cannot be found	The number of suspicious regions incorrectly determined as mass
HCOW	**56**	**2**	**358**
Renyi	54	4	668
Kapur	55	3	788
Shannon	55	3	836

This article has been accepted for publication in a future issue of this journal, but has not been fully edited. Content may change prior to final publication. Citation information: DOI 10.1109/ACCESS.2021.3089077, IEEE Access

According to Table 3, the proposed HCOW method shows the same performance as other methods in finding the mass regions, but its main success is in excluding the regions with no masses. In the table, the number of the suspicious regions that were incorrectly determined as mass by the HCOW method is approximately 46.4% less than the Renyi, 59.6 % less than the Kapur, and 62.2% less than the Shannon methods. These rates reveal the superiority of the proposed method over the other methods when $R \geq 100$. On the other hand, in Table 4, it is seen that the HCOW method found nearly all the masses (only two masses could not be found) while the other methods shown worse performances. Moreover, according to the table, the performance of the HCOW method in decreasing the number of non-masses regions is improved. The numbers of non-mass suspicious regions found by the HCOW method is nearly 46.4% less than the Renyi, 54.5% less than the Kapur, and 57.2% less than the Shannon methods. These results show the effectiveness of both the HCOW method and using an image-specific R value ($R \geq Otsu_{thr}$).

To present a more meaningful evaluation of the results of the second experiment some statistical performance measuring methods were used. The brief descriptions of these methods and of their variables are given as follows [5];

Mass region: The region identified as mass by radiologists.

$True_P$: ROI pixels correctly segmented as ROI pixel (the number of pixels in the mass region that defined as mass by the proposed algorithm)

$True_N$: Non-ROI pixels correctly segmented as non-ROI pixel (the numbers of pixels that located out of the mass region and defined as to be not mass by the proposed algorithm).

$False_P$: Non-ROI pixels segmented as ROI pixel (the numbers of pixels that defined as mass by the proposed algorithm located out of the mass region).

$False_N$: ROI pixels segmented as non-ROI pixel (the numbers of pixels that defined as not mass by the proposed algorithm, but located in the mass region).

$True_P$, $True_N$, $False_P$ and $False_N$ definitions are also depicted in Figure 9.

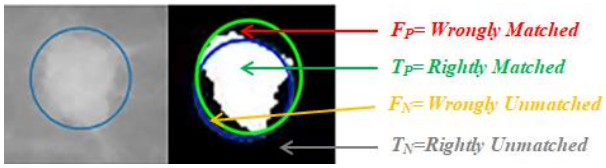

FIGURE 9. Definitions of $True_P$, $True_N$, $False_P$ and $False_N$. Blue Circle represents the boundary that defined by the radiologist while green circle shows the boundary that obtained by the proposed algorithm.

Accuracy: It is "a ratio of the observation of exactly predicted to the whole observations" (the ratio of the accurately determined pixels to all the pixels).

$$Accuracy = \frac{True_P + True_N}{True_P + True_N + False_P + False_N} \times 100 \quad (30)$$

Specificity: It measures "the number of true negatives, which are determined precisely" (the ratio between accurately found pixels of the non-mass region to all the pixels of the non-mass region).

$$Specificity = \frac{True_N}{True_N + False_P} \times 100 \quad (31)$$

False-Positive Rate: It is computed as "the ratio of the count of false-positive predictions to the entire count of negative predictions" (the ratio between pixels that incorrectly determined as mass and all the non-mass pixels)

$$FPR = \frac{False_P}{True_N + False_P} \times 100 \quad (32)$$

Volumetric Overlap (VO): It is the percentage of the pixels in the intersection of segmented region and the ground truth divided by the number of pixels in the union of these two regions. VO is 100 for a perfect segmentation while it is 0 when no overlap at all between the segmentation and the ground truth regions.

$$VO = \frac{|P_{GT} \cap P_S|}{|P_{GT} \cup P_S|} \times 100 \quad (33)$$

Where P_{GT} and P_S represent the number of the pixels in the ground truth and the segmented regions, respectively.

Dice Similarity Coefficient (DSC): It represents the performance of the segmentation algorithm in correctly including the pixels of the ROI inside the segmentation. DSC is 0 when there is no overlap between the segmented region and the ground truth while it is 1 for the perfect segmentation.

$$DSC = \frac{2|P_{GT} \cap P_S|}{|P_{GT}| + |P_S|} \quad (34)$$

The mean values of the accuracy, specificity and FPR are given in Tables 5 and 6 for $R \geq 100$ and $R \geq Otsu_{thr}$, respectively. And, in order to represents the effect of the mammogram-specific R value, the maximum values of VO and DSC are also depicted in the Figure 10 for $R \geq Otsu_{thr}$.

TABLE V
MEAN VALUES OF THE PERFORMANCE MEASURES FOR $R \geq 100$

Performance measures	HCOW	Shannon	Renyi	Kapur
Accuracy	**95,1297**	90,8404	93,2236	92,1728
Specificity	**97,9827**	93,0454	95,6661	94,5118
False Positive Rate	**2,01726**	6,95462	4,33385	5,48822

According to Tables 5 and 6, it is seen that the best results are obtained by the HCOW method for all the performance measures for both of the options of the R value, $R \geq 100$ and $R \geq Otsu_{thr}$. Moreover in Figure 10, it can be seen that the

This article has been accepted for publication in a future issue of this journal, but has not been fully edited. Content may change prior to final publication. Citation information: DOI 10.1109/ACCESS.2021.3089077, IEEE Access

proposed HCOW method with $R \geq Otsu_{thr}$ value obtained the maximum values for both DSC and VO measures over the other methods. And, if we evaluate the results in terms of the $R \geq 100$ and $R \geq Otsu_{thr}$ it can be said that using an adaptive R value improves the performance of the HCOW method by reducing the numbers of the suspicious regions while increasing the finding rate of the masses.

TABLE VI
MEAN VALUES OF THE PERFORMANCE MEASURES FOR $R \geq Otsu_{thr}$

Performance measures	HCOW	Shannon	Renyi	Kapur
Accuracy	**95, 1866**	93,6801	94,9371	94,255
Specificity	**97,8551**	96,2242	97,6799	96,9241
False-Positive Rate	**2,14489**	3,77570	2,32003	3,0758

Finally, it can be said that the HCOW method provides much better results than other methods in accurately determining the mass-regions and in decreasing the rate of the detection of non-mass regions as suspicious regions.

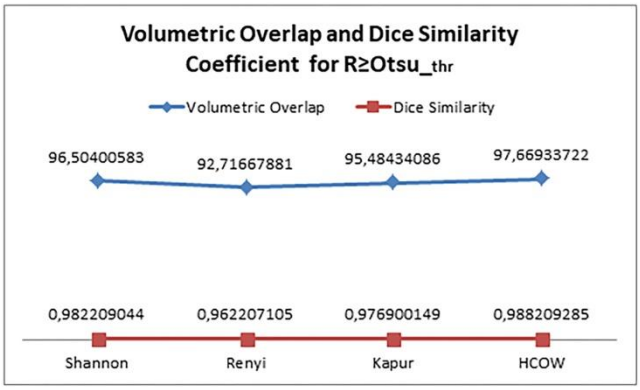

FIGURE 10 Maximum values of VO and DSC for $R \geq Otsu_{thr}$

In addition to compare with the entropy methods, some of the recently published studies that use the same database for the mass segmentation purposes were selected from the literature and their results were compared with the HCOW method, in Table VII. A summary of these methods is as follows; Kurt et al. [49] proposed a novel segmentation method that is based on the Havrda & Charvat and Otsu N thresholding techniques. Kamil and Salih [56] used K-means and Fuzzy C-means algorithms for the segmentation of mammograms . Lbachir et al. [13] developed a four stage CAD system for the classification purpose of the mammograms. And, Shrivastava and Bharti [57] utilized a novel segmentation method based on the region growing and proposed an additional technique for calculating a threshold value for the purpose of region creation in seed region growing.

TABLE VII
COMPARISON OF THE PROPOSED SEGMENTATION METHOD WITH SOME OF THE RELATED STUDIES FROM THE LITERATURE

Works	Year	Accuracy (%)	Specificity (%)	False Positive Rate (%)
Kurt et al. [49]	2014	-	80.6	7.6
Kamil and Salih [56]	2019	91.18(K-mean) 94.12(FCM)	-	-
Lbachir et al. [13]	2020	-	-	2,87 0,467(FPR)
Shrivastava and Bharti [14]	2020	92.2	84.8	15.2
HCOW (Proposed)	2021	95.18	97,98	2,144

According to the table, it can be seen that the HCOW method obtained better results in terms of the accuracy and specificity than the other methods. Moreover, the FPR comparison also shows that the proposed method achieves highly competitive results compared to other methods.

The second experiment was performed on the mass-mammograms. However, an automatic CAD system should accurately classify not only the mass-mammograms, but also the non-mass mammograms. Therefore, the third experiment was performed on 210 non-mass mammograms from the mini-MIAS database. It should be noted that non-mass mammograms can have similar features structurally (dense, oily, glandular) with the mass-mammograms.

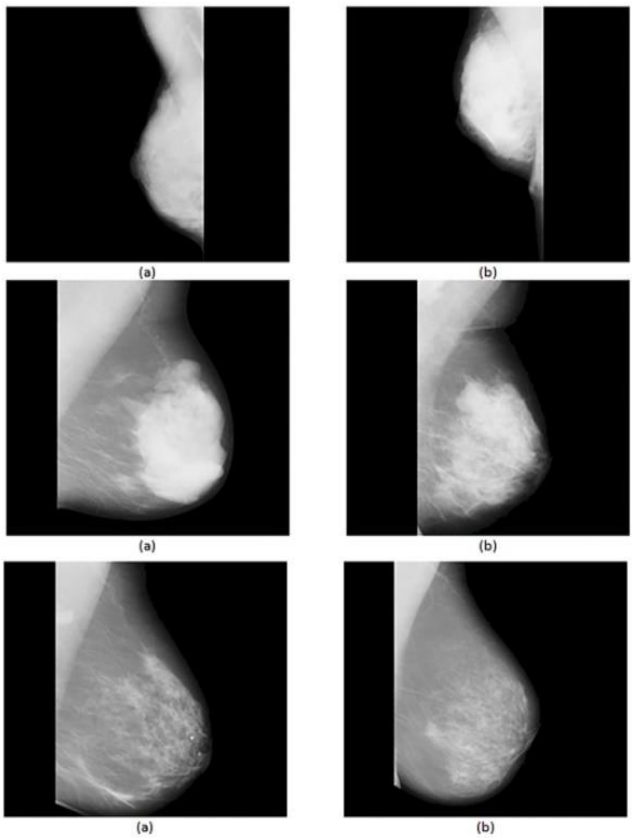

FIGURE 11 Sample mammograms that have similar characteristics to each other a) Non-mass mammograms b) Mass-mammograms

This article has been accepted for publication in a future issue of this journal, but has not been fully edited. Content may change prior to final publication. Citation information: DOI 10.1109/ACCESS.2021.3089077, IEEE Access

Six mammograms that show these similarities are given in Figure 11. In the figure, each row includes two mammograms, one mass-mammogram, and one non-mass mammogram. Both of them have similar characteristics to each other. Hence, a segmentation method can also find suspicious regions on a non-mass mammogram. The proposed method is based on adaptive multi-thresholding and due to the structural similarity between normal and mass-mammograms, it is also possible that there will be suspicious regions found by the HCOW method for normal mammograms. On the other hand, it is expected the system to find as less as possible suspicious regions for a non-mass mammogram. In the third experiment, the 210 non-mass mammograms were segmented by Shannon, Renyi, Kapur and the HCOW methods, and the results were evaluated in terms of the numbers of the determined suspicious regions for all the mammograms. The results were not evaluated according to the performance measures such as accuracy and FPR because there are no mass in the mammograms. In Table 8, the numbers of the suspicious regions for all the methods are given. According to the table , it can be seen that the HCOW method obtained an average of 4.49 suspicious regions per mammogram while the other methods found at least three times higher suspicious regions than the HCOW method.

TABLE VIII
THE NUMBERS OF THE SUSPICIOUS REGIONS OBTAINED FOR NORMAL MAMMOGRAMS

Thresholding methods	The number of mammogram	The number of suspicious regions (ROI)	ROI number per mammogram
HCOW	210	**944**	**4.49**
Shannon	210	3250	15.47
Renyi	210	3135	14.93
Kapur	210	2971	14.14

To visually present the performance of the HCOW method on normal mammograms, four normal mammograms were segmented by the HCOW method and the results are given in Figure 12. In the figure, the normal mammograms, suspicious regions obtained by the HCOW method for these mammograms, and an example cropped ROI from the original mammogram are given. According to the figure it can be seen that there are only a few suspicious regions for each mammogram. It is also seen from the cropped regions that the suspicious regions are obtained only for mass-like regions. These results show that the HCOW method is not only effective in the accurately detection of the mass regions on the mass mammograms, but also effective in determining the suspicious regions for non-mass mammograms.

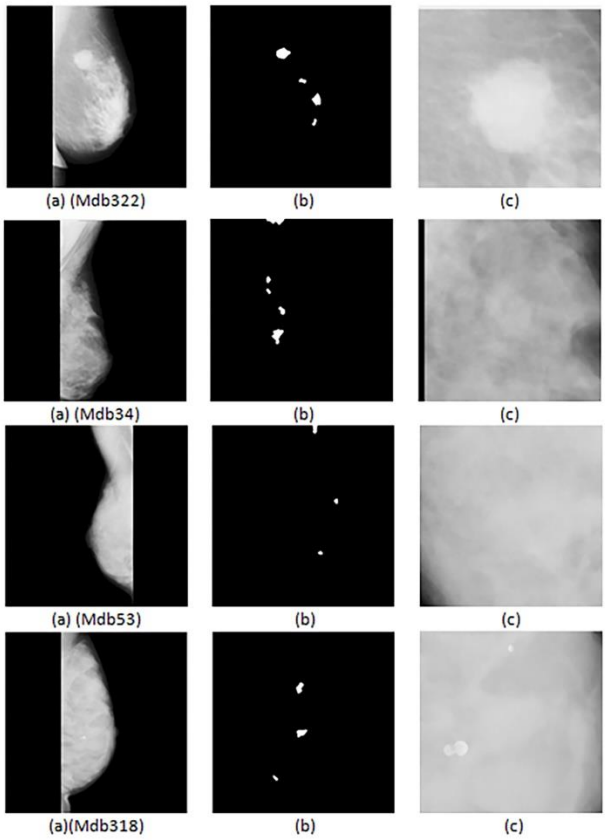

FIGURE 12 Normal mammograms that have different characteristics and their suspicious regions determined by the HCOW method. (a) Original Mammograms (b) Obtained ROI by the HCOW method (c) Cropped ROI of the original mammogram

IV. CONCLUSION

In this study, a new hybrid, fully-automatic thresholding method was proposed to detect suspicious regions on mammograms. The proposed method is based on using three different techniques together, the w-BSAFCM algorithm, the Otsu multilevel thresholding, and the Havrda & Charvat entropy methods. The method handles the entire mammogram in two sub-images, the pectoral muscle, and the breast region and performs segmentation on both of these two images to prevent any information loss. The proposed method was tested on 55 mass mammograms and 210 non-mass mammograms that were taken from the mini-MIAS database. The results of the experiments were evaluated according to the number of determined suspicious regions, the number of the correctly detected masses, and several performance measures and compared with, Shannon, Renyi and Kapur entropy methods and with some of the related studies from the literature. According to the results, it was shown that the proposed method gives better results for almost all parameters than the compared methods. In future studies, the proposed method will be integrated with the classification techniques to be selected to obtain a fully-automatic CAD system for breast cancer diagnosis.

REFERENCES

[1] "world health organization." [Online]. Available: https://www.who.int/news-room/fact-sheets/detail/cancer. [Accessed: 19-Nov-2020].

[2] L. Wang, "Early diagnosis of breast cancer," *Sensors (Switzerland)*, vol. 17, no. 7, 2017.

[3] E. U. Ekpo, M. Alakhras, and P. Brennan, "Errors in mammography cannot be solved through technology alone," *Asian Pacific Journal of Cancer Prevention*, vol. 19, no. 2. Asian Pacific Organization for Cancer Prevention, pp. 291–301, 01-Feb-2018.

[4] R. Masud, M. Al-Rei, and C. Lokker, "Computer-aided detection for breast cancer screening in clinical settings: Scoping review," *Journal of Medical Internet Research*, vol. 21, no. 7. Journal of Medical Internet Research, 01-Jul-2019.

[5] M. Moghbel, C. Y. Ooi, N. Ismail, Y. W. Hau, and N. Memari, "A review of breast boundary and pectoral muscle segmentation methods in computer-aided detection/diagnosis of breast mammography," *Artif. Intell. Rev.*, vol. 53, no. 3, pp. 1873–1918, Mar. 2020.

[6] S. Beura, B. Majhi, and R. Dash, "Mammogram classification using two dimensional discrete wavelet transform and gray-level co-occurrence matrix for detection of breast cancer," *Neurocomputing*, vol. 154, pp. 1–14, Apr. 2015.

[7] N. Gedik, "A new feature extraction method based on multi-resolution representations of mammograms," *Appl. Soft Comput.*, vol. 44, pp. 128–133, 2016.

[8] I. Wichakam and P. Vateekul, "Combining deep convolutional networks and SVMs for mass detection on digital mammograms," in *2016 8th International Conference on Knowledge and Smart Technology, KST 2016*, 2016, pp. 239–244.

[9] S. R. T. J. Goubalan, Y. Goussard, and H. Maaref, "Unsupervised malignant mammographic breast mass segmentation algorithm based on pickard Markov random field," in *Proceedings - International Conference on Image Processing, ICIP*, 2016, vol. 2016-Augus, pp. 2653–2657.

[10] Vedanarayanan V and N. Nm, "Advanced image segmentation techniques for accurate isolation of abnormality to enhance breast cancer detection in digital mammographs," Allied Academies, Mar. 2017.

[11] S. Boudraa, A. Melouah, and H. F. Merouani, "Improving mass discrimination in mammogram-CAD system using texture information and super-resolution reconstruction," *Evol. Syst.*, vol. 11, no. 4, pp. 697–706, Dec. 2020.

[12] D. Lévy and A. Jain, "Breast Mass Classification from Mammograms using Deep Convolutional Neural Networks," no. Nips, 2016.

[13] I. A. Lbachir, I. Daoudi, and S. Tallal, "Automatic computer-aided diagnosis system for mass detection and classification in mammography," *Multimed. Tools Appl.*, pp. 1–33, Nov. 2020.

[14] N. Shrivastava and J. Bharti, "Breast tumor detection and classification based on density," *Multimed. Tools Appl.*, vol. 79, no. 35, pp. 26467–26487, Jul. 2020.

[15] K. U. Sheba and S. Gladston Raj, "An approach for automatic lesion detection in mammograms," *Cogent Eng.*, vol. 5, no. 1, Mar. 2018.

[16] S. Sharma and P. Khanna, "Computer-Aided Diagnosis of Malignant Mammograms using Zernike Moments and SVM," *J. Digit. Imaging*, vol. 28, no. 1, pp. 77–90, 2014.

[17] B. Sridhar, K. V. V. S. Reddy, and A. M. Prasad, "Mammographic image analysis based on adaptive morphological fuzzy logic CAD system," *Int. J. Biomed. Eng. Technol.*, vol. 17, no. 4, pp. 341–355, 2015.

[18] H. Samma, C. P. Lim, and A. Samma, "A computer-aided detection system for automatic mammography mass identification," in *Lecture Notes in Computer Science (including subseries Lecture Notes in Artificial Intelligence and Lecture Notes in Bioinformatics)*, 2010, vol. 6444 LNCS, no. PART 2, pp. 226–233.

[19] A. Elmoufidi, K. El Fahssi, S. Jai-andaloussi, A. Sekkaki, Q. Gwenole, and M. Lamard, "Anomaly classification in digital mammography based on multiple-instance learning," *IET Image Process.*, vol. 12, no. 3, pp. 320–328, Mar. 2018.

[20] A. Akselrod-Ballin, L. Karlinsky, S. Alpert, S. Hashoul, R. Ben-Ari, and E. Barkan, "A CNN based method for automatic mass detection and classification in mammograms," *Comput. Methods Biomech. Biomed. Eng. Imaging Vis.*, vol. 7, no. 3, pp. 242–249, May 2019.

[21] D. A. Zebari, D. Q. Zeebaree, A. M. Abdulazeez, H. Haron, and H. N. A. Hamed, "Improved threshold based and trainable fully automated segmentation for breast cancer boundary and pectoral muscle in mammogram images," *IEEE Access*, vol. 8, pp. 1–20, 2020.

[22] V. K. Singh *et al.*, "Breast tumor segmentation and shape classification in mammograms using generative adversarial and convolutional neural network," *Expert Syst. Appl.*, vol. 139, p. 112855, 2020.

[23] R. S. Patil and N. Biradar, "Improved region growing segmentation for breast cancer detection: progression of optimized fuzzy classifier," *Int. J. Intell. Comput. Cybern.*, vol. 13, no. 2, pp. 181–205, 2020.

[24] K. A. Santhos, A. Kumar, V. Bajaj, and G. K. Singh, "McCulloch's algorithm inspired cuckoo search optimizer based mammographic image segmentation," *Multimed. Tools Appl.*, vol. 79, no.

41–42, pp. 30453–30488, 2020.

[25] S. El Idrissi El Kaitouni, A. Abbad, and H. Tairi, "A breast tumors segmentation and elimination of pectoral muscle based on hidden markov and region growing," *Multimed. Tools Appl.*, vol. 77, no. 23, pp. 31347–31362, 2018.

[26] B. Gupta and M. Tiwari, "A tool supported approach for brightness preserving contrast enhancement and mass segmentation of mammogram images using histogram modified grey relational analysis," *Multidimens. Syst. Signal Process.*, vol. 28, no. 4, pp. 1549–1567, 2017.

[27] L. Ahmed, M. M. Iqbal, H. Aldabbas, S. Khalid, Y. Saleem, and S. Saeed, "Images data practices for Semantic Segmentation of Breast Cancer using Deep Neural Network," *J. Ambient Intell. Humaniz. Comput.*, no. 0123456789, 2020.

[28] T.-S. K. Mugahed A. Al-antari, Mohammed A. Al-masni, Mun-Taek Choi, Seung-Moo Han, "A fully integrated computer-aided diagnosis system for digital X-ray mammograms via deep learning detection, segmentation, and classification," *Informatics, Int. J. Med.*, vol. 117, pp. 44–54, 2018.

[29] N. Otsu, "A threshold selection method from gray-level histograms," *IEEE Trans Syst Man Cybern*, vol. SMC-9, no. 1, pp. 62–66, 1979.

[30] B. Singh Khehra and A. P. Singh Pharwaha, "Digital mammogram segmentation using non-Shannon measures of entropy," in *Proceedings of the World Congress on Engineering 2011, WCE 2011*, 2011, vol. 2, pp. 1634–1640.

[31] G. Toz, İ. Yücedağ, and P. Erdoğmuş, "A fuzzy image clustering method based on an improved backtracking search optimization algorithm with an inertia weight parameter," *J. King Saud Univ. - Comput. Inf. Sci.*, vol. 31, no. 3, pp. 295–303, Jul. 2019.

[32] P. Civicioglu, "Backtracking Search Optimization Algorithm for numerical optimization problems," *Appl. Math. Comput.*, vol. 219, no. 15, pp. 8121–8144, Apr. 2013.

[33] J. C. Bezdek, R. Ehrlich, and W. Full, "FCM: The fuzzy c-means clustering algorithm," *Comput. Geosci.*, vol. 10, no. 2–3, pp. 191–203, Jan. 1984.

[34] "The mini-MIAS database of mammograms." [Online]. Available: http://peipa.essex.ac.uk/info/mias.html. [Accessed: 05-Dec-2020].

[35] V. Vijikala and D. A. S. Dhas, "Identification of most preferential denoising method for mammogram images," 2016, pp. 173–179.

[36] M. Kumar, V. M. Thakkar, H. S. Bhadauria, and I. Kumar, "Mammogram's denoising in spatial and frequency domain," in *Proceedings on 2016 2nd International Conference on Next Generation Computing Technologies, NGCT 2016*, 2017, pp. 654–659.

[37] A. Mencattini, M. Salmeri, R. Lojacono, M. Frigerio, and F. Caselli, "Mammographic images enhancement and denoising for breast cancer detection using dyadic wavelet processing," *IEEE Trans. Instrum. Meas.*, vol. 57, no. 7, pp. 1422–1430, 2008.

[38] J. K. Kim, J. M. Park, K. S. Song, and H. W. Park, "Adaptive mammographic image enhancement using first derivative and local statistics," *IEEE Trans. Med. Imaging*, vol. 16, no. 5, pp. 495–502, 1997.

[39] S. Amutha, D. R. Ramesh Babu, M. Ravi Shankar, and N. Harish Kumar, "Mammographic image enhancement using modified mathematical morphology and Bi-orthogonal wavelet," in *ITME 2011 - Proceedings: 2011 IEEE International Symposium on IT in Medicine and Education*, 2011, vol. 1, pp. 548–553.

[40] H. Moradmand, S. Setayeshi, A. R. Karimian, M. Sirous, and M. E. Akbari, "Comparing the performance of image enhancement methods to detect microcalcification clusters in digital mammography," *Iran. J. Cancer Prev.*, vol. 5, no. 2, pp. 61–68, 2012.

[41] K. Akila, L. S. Jayashree, and A. Vasuki, "Mammographic image enhancement using indirect contrast enhancement techniques - A comparative study," in *Procedia Computer Science*, 2015, vol. 47, no. C, pp. 255–261.

[42] J. Weickert and B. G. T. Stuttgart, "Anisotropic Diffusion in Image Processing."

[43] Deepa S and SubbiahBharathi V, "Efficient ROI Segmentation of Digital Mammogram Images using Otsu's N thresholding method," IJERT-International Journal of Engineering Research & Technology, Jan. 2013.

[44] S. Sharma and P. Khanna, "ROI segmentation using Local Binary Image," in *Proceedings - 2013 IEEE International Conference on Control System, Computing and Engineering, ICCSCE 2013*, 2013, pp. 136–141.

[45] D. Cascio *et al.*, "Mammogram segmentation by contour searching and mass lesions classification with neural network," *IEEE Trans. Nucl. Sci.*, vol. 53, no. 5, pp. 2827–2833, Oct. 2006.

[46] B. W. Hong and B. S. Sohn, "Segmentation of regions of interest in mammograms in a topographic approach," in *IEEE Transactions on Information Technology in Biomedicine*, 2010, vol. 14, no. 1, pp. 129–139.

[47] J. Nagi, S. Abdul Kareem, F. Nagi, and S. Khaleel Ahmed, "Automated breast profile segmentation for ROI detection using digital mammograms," in *Proceedings of 2010 IEEE EMBS Conference on Biomedical Engineering and Sciences, IECBES 2010*, 2010, pp. 87–92.

[48] F. Fauci *et al.*, "Mammogram segmentation by

contour searching and massive lesion classification with neural network," in *IEEE Nuclear Science Symposium Conference Record*, 2004, vol. 5, pp. 2695–2699.

[49] B. Kurt, V. V. Nabiyev, and K. Turhan, "A novel automatic suspicious mass regions identification using Havrda & Charvat entropy and Otsu's N thresholding," *Comput. Methods Programs Biomed.*, vol. 114, no. 3, pp. 349–360, May 2014.

[50] G. H. Rauscher, E. F. Conant, J. A. Khan, and M. L. Berbaum, "Mammogram image quality as a potential contributor to disparities in breast cancer stage at diagnosis: an observational study," *BMC Cancer*, vol. 13, p. 208, Apr. 2013.

[51] R. J. Ferrari, R. M. Rangayyan, J. E. L. Desautels, R. A. Borges, and A. F. Frère, "Automatic Identification of the Pectoral Muscle in Mammograms," *IEEE Trans. Med. Imaging*, vol. 23, no. 2, pp. 232–245, Feb. 2004.

[52] A. Sultana, M. Ciuc, and R. Strungaru, "Detection of pectoral muscle in mammograms using a mean-shift segmentation approach," in *2010 8th International Conference on Communications, COMM 2010*, 2010, pp. 165–168.

[53] S. M. Kwok, R. Chandrasekhar, and Y. Attikiouzel, "Automatic pectoral muscle segmentation on mammograms by straight line estimation and cliff detection," in *ANZIIS 2001 - Proceedings of the 7th Australian and New Zealand Intelligent Information Systems Conference*, 2001, pp. 67–72.

[54] W. Xu, H. Li, and W. Liu, "A novel pectoral muscle segmentation algorithm based on polyline fitting and elastic thread approaching," in *2007 1st International Conference on Bioinformatics and Biomedical Engineering, ICBBE*, 2007, pp. 837–840.

[55] G. Toz and P. Erdogmus, "A Single Sided Edge Marking Method for Detecting Pectoral Muscle in Digital Mammograms," 2018.

[56] M. Y. Kamil and A. M. Salih, "Mammography images segmentation via Fuzzy C-mean and K-mean," *Int. J. Intell. Eng. Syst.*, vol. 12, no. 1, pp. 22–29, 2019.

Güliz Toz received the M.S. degrees from the Electrical-Electronic Engineering and the Ph.D. degrees from the Electrical-Electronic and Computer Engineering Duzce University, Duzce, Turkey, in 2014 and 2018, respectively. Her research interests include medical image processing, machine learning, and optimization. She is currently working as a lecturer at Karamanoğlu Mehmetbey University.

Dr. Pakize ERDOGMUS received the B.S. degree in Electronic and Communication Engineering from Yıldız Technical University, Kocaeli Engineering Faculty, M. S degree in Computer Sciences and Ph.D degree on Numerical Methods from Ataturk University. Her research interests include Digital Image Processing, Nature Inspired-Optimization Algorithms and Computational Intelligence.